Robotica (2013) volume 31, pp. 1119–1129. © Cambridge University Press 2013
doi:10.1017/S0263574713000362

Minimum control effort trajectory planning and tracking of the CEDRA brachiation robot

Ali Meghdari*, Seyyed Mohammad H. Lavasani, Mohsen Norouzi and Mir Saman Rahimi Mousavi

Center of Excellence in Design, Robotics and Automation (CEDRA), School of Mechanical Engineering, Sharif University of Technology, Tehran, Iran

(Accepted April 9, 2013. First published online: May 14, 2013)

SUMMARY

The control of a brachiation robot has been the primary objective of this study. A brachiating robot is a type of a mobile arm that is capable of moving from branch to branch similar to a long-armed ape. In this paper, to minimize the actuator work, Pontryagin's minimum principle was used to obtain the optimal trajectories for two different problems. The first problem considers "brachiation between fixed branches with different distance and height," whereas the second problem deals with the "brachiating and catching of a moving target branch". Theoretical results show that the control effort in the proposed method is reduced by 25% in comparison with the "target dynamics" method which was proposed by Nakanishi *et al.* (1998)[16] for the same type of robot. As a result, the obtained optimal trajectory also minimizes the brachiation time. Two kinds of controllers, namely the proportional-derivative (PD) and the adaptive robust (AR), were investigated for tracking the proposed trajectories. Then, the previous method on a set-point controller for acrobat robots is improved to represent a new AR controller which allows the system to track the desired trajectory. This new controller has the capability to be used in systems which have uncertainties in the kinematic and dynamic parameters. Finally, theoretical results are presented and validated with experimental observations with a PD controller due to the no chattering phenomenon and small computational efforts.

KEYWORDS: Brachiation robot; Minimum effort optimal control; Irregular ladder; Moving target bar; Adaptive robust tracking control; PD tracking control.

1. Introduction

During the late 1990s, a new type of robotic mechanism was introduced by Fukuda and coworkers.[1] The proposed mechanism consists of a two-link underactuated brachiating robot called Brachiator, which in appearance imitates the movement of an ape swinging from branch to branch. The swinging motion of an ape is shown in Fig. 1. Unlike other robots where the gravity force is one of the difficulties which reduce the stability of the system, gravity helps this robot to use minimum control effort to move from one branch to another.[2]

The applications of brachiation robots are considerable. These robots can be used in the inspection and repair of power transmission lines and cable-stayed bridge,[3,4] which are dangerous tasks for human beings.

A brachiating robot with 2 degrees of freedom and a single actuator is a clear example of an underactuated system. Underactuated systems are those for which the number of actuators within the system is less than their degrees of freedom. The control issue of underactuated mechanical systems is a research topic that has been studied extensively during the past few years. Some examples are unmanned aerial vehicles (UAVs),[5,6] flexible manipulators,[7] swing up of acrobat robot,[8] cart-pole or rotating pendulum,[9] inertia wheel pendulum, and wheeled mobile robot.

Thus far, different methods have been used to control a brachiation robot. In 1991, Fukuda *et al.*[10] used a heuristic method to propose the time sequence of control inputs with no a priori knowledge of the robot's dynamics. They used the interpolation of a cerebellar model arithmetic computer to estimate the time sequence of control inputs for unexperienced conditions. Two feedback controllers, namely the trajectory feedback control and the arm-direction feedback control, were used to achieve more robustness.[10–12]

Gomes *et al.*[13] used numerical integration and root-finding to form an absolute zero energy cost motion for brachiating of the brachiation robot. They sought an initial condition that ensures that the end-effector of the robot reaches the target bar with zero relative velocity. Hence, there is no energy loss when the robot's hand comes into contact with the handhold. Their solutions to the problem do not require any joint torque at any period of time. They repeated this approach for a brachiation robot with two, three and five links and with 7 degrees of freedom in ricochetal brachiation.

Another work was done by Nishimura *et al.*[14,15] to utilize final-state control with error learning to achieve feed-forward input in order to bring the three-link brachiation robot from an initial state to a desired state in a specific time. In their papers, the brachiation robot is treated as a discrete-time linear parameter-varying system.[14,15]

One of the important works done in this field is known as the "target dynamics" method.[1] The target dynamics method is an example of input/output linearization with

* Corresponding author. E-mail: Meghdari@sharif.edu

https://doi.org/10.1017/S0263574713000362 Published online by Cambridge University Press

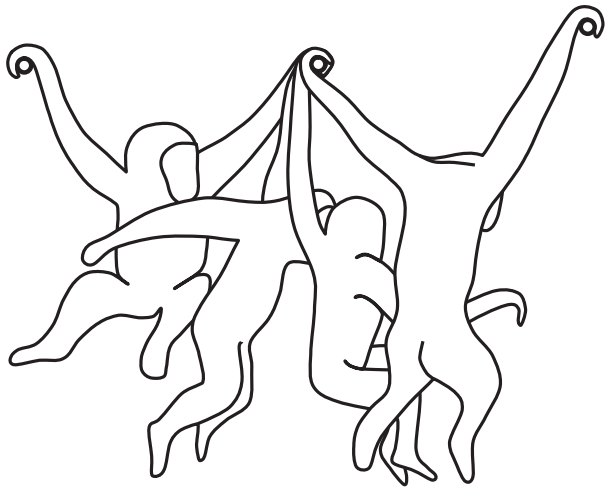


Fig. 1. Brachiation of the long-armed ape on uneven supports.

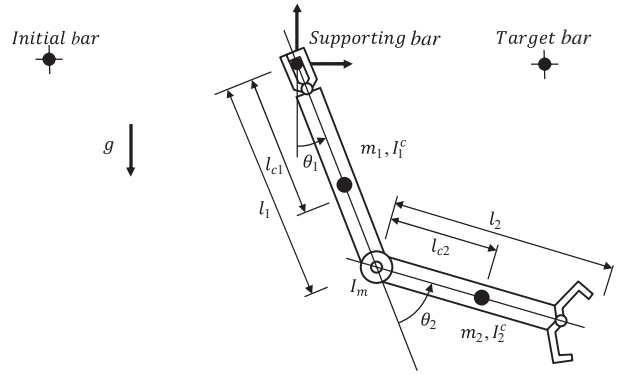


Fig. 2. Kinematic and dynamic parameters and generalized coordinate of the simplified brachiation robot.

a feed-forward controller. Nakanishi *et al.*[1,16–19] inverted the dynamics of the brachiation robot and changed its characteristic to behave as a specified target dynamical system. They stated that biomechanical studies show that slow brachiating of an ape is like motion of a 1 degree-of-freedom pendulum. Hence, they concluded that this mechanism like the target dynamics requires less energy for its motion. They developed a numerical method to obtain "virtual frequency" of a 1 degree-of-freedom pendulum to make the system reach the desired state. This work was extended to brachiate between branches with irregular intervals but at the same height.[20] Here, the results of the "target dynamics" method and the optimal method are presented. Theoretical results show that the control effort in the proposed method (optimal control) is reduced by 25% in comparison with the "target dynamics" method.

De Olivera *et al.*[3,4,21] used nonlinear model-based predictive control (NMPC) and linear MPC to propose a method to control a three-link brachiation robot. The MPC method was used because it could deal with constraints on inputs and state and presented an optimal control law. This paper investigates two new problems related to the control of brachiation robots. The first problem considers "brachiation between fixed branches with different distance and height" and the second deals with the "brachiating and catching of the moving target branch".

The paper is organized as follows. In Section 2, the governing equations of motion of the brachiation robot are achieved. The objective is to find optimal trajectories for reducing the control effort and brachiation time in comparison with previous trajectories used for this robot. Therefore, in Section 3, for the two listed problems, optimal trajectories are investigated based on Pontryagin's minimum principle. Furthermore, simulation results are shown and compared with other published works. Due to the existence of disturbances and uncertainties in the system's model, a feed-forward controller (optimal control) by itself cannot be applied to the brachiation robot. Hence, in Section 4, two kinds of tracking controllers, the proportional-derivative (PD) and the adaptive robust (AR), are presented. Then, simulation results are compared and discussed in the presence of model uncertainties. In Section 5, the experimental setup is exposed and the results are presented.

2. Problem Setup

The simplified model for the brachiation robot is a planar double pendulum which is actuated at the elbow joint. The parameters and the generalized coordinate of the system, which are used to obtain the optimal trajectory and tracking controller for the system, are shown in Fig. 2.

The Euler–Lagrange equation is used to obtain the differential equation-of-motion of the system. The Lagrangian of the system is

$$\mathcal{L} = \mathcal{K} - \mathcal{U} = \frac{1}{2}\dot{\boldsymbol{q}}^T \boldsymbol{M}(\boldsymbol{q})\dot{\boldsymbol{q}} - \mathcal{U}(\boldsymbol{q}), \tag{1}$$

where $\mathcal{K}$ is the kinetic energy and $\mathcal{U}$ is the potential energy of the system. $\boldsymbol{M}(\boldsymbol{q}) \in \mathbb{R}^{n\times n}$ is the inertia matrix which is a symmetric positive-definite matrix and $\boldsymbol{q} = [\theta_1, \theta_2]^T \in \mathbb{R}^n$ is the generalized coordinate and represents the joint position. In this robot, n equals 2. The Euler–Lagrange equation states that

$$\frac{d}{dt}\left(\frac{\partial \mathcal{L}}{\partial \dot{\boldsymbol{q}}_i}\right) - \frac{\partial \mathcal{L}}{\partial \boldsymbol{q}_i} = \mathcal{F}_i, \tag{2}$$

where $\mathcal{F} \in \mathbb{R}^n$ is the vector of the applied joint torque to the system. Using Eq. (1), the equation-of-motion of the system is obtained as

$$\boldsymbol{M}(\boldsymbol{q})\ddot{\boldsymbol{q}} + \boldsymbol{C}(\boldsymbol{q}, \dot{\boldsymbol{q}})\dot{\boldsymbol{q}} + \boldsymbol{G}(\boldsymbol{q}) + \boldsymbol{D}(\boldsymbol{q}, \dot{\boldsymbol{q}}) = \mathcal{F}, \tag{3}$$

where $\boldsymbol{C}(\boldsymbol{q}, \dot{\boldsymbol{q}}) \in \mathbb{R}^{n\times n}$ is the matrix of the centrifugal and Coriolis terms, $\boldsymbol{G}(\boldsymbol{q}) \in \mathbb{R}^n$ represents the vector of gravitational forces and $\boldsymbol{D}(\boldsymbol{q}, \dot{\boldsymbol{q}}) \in \mathbb{R}^n$ is the vector of the friction coefficient of the joints. By selecting the matrix $\boldsymbol{C}(\boldsymbol{q}, \dot{\boldsymbol{q}})$ appropriately, it can be readily concluded that the matrix $\dot{\boldsymbol{M}}(\boldsymbol{q}) - 2\boldsymbol{C}(\boldsymbol{q}, \dot{\boldsymbol{q}})$ is skew-symmetric. Because the system is underactuated, the vector of the applied joint torque has the form:

$$\mathcal{F} = \begin{bmatrix} 0 \\ \tau \end{bmatrix}, \tag{4}$$

https://doi.org/10.1017/S0263574713000362 Published online by Cambridge University Press

where τ is the exerted torque to link 2 from link 1 and it is produced by the central actuator. Moreover, the first row of Eq. (3) can be expressed as a second-order differential equation:

$$\varphi(\ddot{\boldsymbol{q}}, \dot{\boldsymbol{q}}, \boldsymbol{q}) = 0, \tag{5}$$

which contains Coriolis, centrifugal, friction and gravity terms that can be highly nonlinear. In such systems, Eq. (5) appears as a second-order nonholonomic constraint. This constraint is a function of kinematic and dynamic parameters and the objective here is to find proper trajectories to satisfy this constraint.

The inertia matrix, the matrix of centrifugal and coriolis terms, the vector of gravitational effect and the vector of the friction coefficient are considered as

$$\begin{aligned}
\boldsymbol{M}(\boldsymbol{q}) &= \begin{bmatrix} a_1 + a_2 + 2a_3\cos(q_2) & a_2 + a_3\cos(q_2) \\ a_2 + a_3\cos(q_2) & a_2 + I_m \end{bmatrix}, \\
\boldsymbol{C}(\boldsymbol{q}, \dot{\boldsymbol{q}}) &= -a_3\sin(q_2) \begin{bmatrix} \dot{q}_2 & \dot{q}_1 + \dot{q}_2 \\ -\dot{q}_1 & 0 \end{bmatrix}, \\
\boldsymbol{G}(\boldsymbol{q}) &= \begin{bmatrix} b_1\sin(q_2) + b_2\sin(q_1 + q_2) \\ b_2\sin(q_1 + q_2) \end{bmatrix}, \\
\boldsymbol{D}(\boldsymbol{q}, \dot{\boldsymbol{q}}) &= \begin{bmatrix} c_1\mathrm{sign}(\dot{q}_1) + \nu_1\dot{q}_1 \\ c_2\mathrm{sign}(\dot{q}_2) + \nu_2\dot{q}_2 \end{bmatrix},
\end{aligned} \tag{6}$$

where

$$\begin{aligned}
&a_1 = m_1 l_{c1}^2 + m_2 l_1^2 + I_1^c, \quad a_2 = m_2 l_{c2}^2 + I_2^c, \quad a_3 = m_2 l_1 l_{c2}, \\
&b_1 = (m_1 l_{c1} + m_2 l_1) g, \quad b_2 = m_2 l_{c2} g,
\end{aligned} \tag{7}$$

where m_i, l_i and l_{ci} are the mass, length and center of mass of link i, respectively. I_i^c is the moment of inertia of the link i about an axis perpendicular to the plane of motion at the center of mass, and I_m is the equivalent moment of inertia of the moving parts (rotor and gears) of the actuator. c_i and ν_i are the Coulomb friction and viscous damping coefficient of the joint i, and g is the gravitational acceleration. Kinematic and dynamic parameters of the brachiation robot for the first swing from which link 1 is suspended from the supporting bar are mentioned in Table I, where the mass and length of each link are obtained by direct measurements and the centers of mass are estimated by the balancing method. To measure the two moments of inertia and the first viscous damping coefficient, the two links of the brachiation robot were taken apart and a simple system identification method was used based on an observation of the vibration of each link about its pivot. The moments of inertia are found from the natural frequency of the mentioned vibration, while the first viscous damping coefficient is obtained from the logarithmic decrement of the amplitude of the link vibration. At last, the second friction coefficients and I_m are acquired from actuator datasheets.

Then, the state space model of the system is introduced as

$$\dot{\boldsymbol{x}}(t) = \boldsymbol{f}(\boldsymbol{x}(t), \boldsymbol{u}(t), t), \tag{8}$$

Table I. Kinematic and dynamic parameters of the CEDRA brachiation robot.

Symbols (unit)	$i = 1$	$i = 2$
m_i (kg)	0.545	1.270
l_i (m)	0.262	0.262
l_{ci} (m)	0.123	0.067
I_i^c (kgm^2)	$3.6e-3$	$9.6e-3$
c_i (N m)	0	0.1
ν_i (N m s)	0.02	0.02
I_m (kg m^2)	$2.5e-3$	

where $\boldsymbol{x}(t)$ and $\boldsymbol{u}(t)$ are

$$\begin{aligned}
\boldsymbol{x} &= [\boldsymbol{x}_1, \boldsymbol{x}_2]^T = [\boldsymbol{q}, \dot{\boldsymbol{q}}]^T \in \mathbb{R}^{2n}, \\
\boldsymbol{u} &= \begin{bmatrix} 0 \\ \tau \end{bmatrix}.
\end{aligned} \tag{9}$$

3. Optimal Trajectory Planning

This section considers and discusses the issue of designing an optimal trajectory for a brachiation robot. The theoretical results obtained here indicate that the control effort is reduced in comparison with the "target dynamics" method, which was proposed in prior papers for such a robot. For the sake of analysis, the problem is broken down into two parts as P1 and P2:

P1: Brachiation between fixed branches with different distance and height.
P2: Brachiating and catching of the moving target branch.

3.1. The P1 statement

In this part, it is assumed that the branches are fixed at irregular intervals and their position is known. The objective here is to find a global minimum for the following functional:

$$J(\boldsymbol{x}(t), \boldsymbol{u}(t), t) = \frac{1}{2}\boldsymbol{e}_p(t_f)^2_{\boldsymbol{R}1} + \frac{1}{2}\boldsymbol{e}_v(t_f)^2_{\boldsymbol{R}2} + \int_{t_0}^{t_f} \left\{K + \boldsymbol{u}^2_{\boldsymbol{R}3}\right\} dt, \tag{10}$$

where

$$\begin{aligned}
\boldsymbol{e}_p(t_f) &= \boldsymbol{x}_1(t_f) - \boldsymbol{x}_{1f}, \\
\boldsymbol{e}_v(t_f) &= \boldsymbol{x}_2(t_f) - \boldsymbol{x}_{2f},
\end{aligned} \tag{11}$$

where t_0 and t_f are the initial and final times of the brachiation, respectively, and $\boldsymbol{e}^2_{\boldsymbol{R}}$ means $\boldsymbol{e}^T\boldsymbol{R}\boldsymbol{e}$. The functional $J(\boldsymbol{x}(t), \boldsymbol{u}(t), t)$ is the performance criterion, and $\boldsymbol{R}1$, $\boldsymbol{R}2$ and $\boldsymbol{R}3$ are the positive-definite matrices. In addition, the desired goal is also to minimize the brachiation time. Hence, the boundary for t_f is considered as a free boundary. The parameter $K \geq 0$ is a design parameter, which when changes has an effect on the ratio of t_f to maximum of the

https://doi.org/10.1017/S0263574713000362 Published online by Cambridge University Press

applied torque. The initial and final boundary conditions are

$$\boldsymbol{x}_0 = \begin{bmatrix} \theta_{10} \\ \theta_{20} \\ 0 \\ 0 \end{bmatrix}, \boldsymbol{x}_f = \begin{bmatrix} \theta_{1f} \\ \theta_{2f} \\ 0 \\ 0 \end{bmatrix}. \tag{12}$$

The joints position of the brachiation robot is obtained by inverse kinematics methods. The final angular velocities of each joint are assumed to be zero for a smooth approach to the target bar. It should be noted that this assumption is very important for extending "P1" to "continuous contact brachiation on uneven fixed supports", without any energy losses due to collisions of the end-effector with the target bar. The coefficient of restitution is[22]

$$e = -\frac{v_{en}^2 - v_{bn}^2}{v_{en}^1 - v_{bn}^1}, \tag{13}$$

where v_{en} and v_{bn} are the components of the velocities of the end-effector and the target bar, normal to the collision surface and superscripts 1 and 2 refer to "just before" and "after impact". In the P1 problem, the target bar is fixed, meaning $v_{bn}^1 = v_{bn}^2 = 0$, and $v_{en}^2 = 0$ after the final impact with the fixed target bar. Therefore,

$$ev_{en}^1 = 0. \tag{14}$$

When $e = 1$, the collision is a perfectly elastic impact and there is no energy dissipation. This leads to

$$\begin{bmatrix} \dot{\theta}_{1f} \\ \dot{\theta}_{2f} \end{bmatrix} = \begin{bmatrix} 0 \\ 0 \end{bmatrix}. \tag{15}$$

3.2. The P2 statement

In this part, it is assumed that the target bar is movable and its path is known or can be predicted. The objective here is to find a global minimum for the functional in Eq. (10). With the initial conditions set as

$$\boldsymbol{x}_0 = \begin{bmatrix} \theta_{10} \\ \theta_{20} \\ 0 \\ 0 \end{bmatrix}, \tag{16}$$

the final state lies on the known moving point, as a function of time:

$$\boldsymbol{x}_1 = \boldsymbol{m}(t) \in \mathbb{R}^n \Rightarrow \boldsymbol{x}_{1f} = \boldsymbol{m}(t_f), \boldsymbol{x}_{2f} = \dot{\boldsymbol{m}}(t_f). \tag{17}$$

Therefore, the final time is also a free boundary and has to minimize.

3.3. Necessary conditions for optimality for P1

In order to determine the necessary conditions for optimality, the costate vector $\boldsymbol{p}(t) \in \mathbb{R}^{2n}$ of the Hamiltonian function can be defined as follows:[23]

$$\mathcal{H}(\boldsymbol{x}(t), \boldsymbol{u}(t), \boldsymbol{p}(t), t) \triangleq g(\boldsymbol{x}(t), \boldsymbol{u}(t), t) + \boldsymbol{p}^T(t)[\boldsymbol{f}(\boldsymbol{x}(t), \boldsymbol{u}(t), t)]. \tag{18}$$

The performance criterion functional has the general form as follows:

$$J(\boldsymbol{x}(t), \boldsymbol{u}(t), t) = h(\boldsymbol{x}(t_f), t_f) + \int_{t_0}^{t_f} g(\boldsymbol{x}(t), \boldsymbol{u}(t), t)dt, \tag{19}$$

where $h(\boldsymbol{x}(t_f), t_f)$ and $g(\boldsymbol{x}(t), \boldsymbol{u}(t), t)$ are scalar functions. $h(\boldsymbol{x}(t_f), t_f)$ is the differentiable function of time and $g(\boldsymbol{x}(t), \boldsymbol{u}(t), t)$ has continuous first and second partial derivatives with respect to all of its argument. Pontryagin's minimum principle states that there exists a nonzero costate vector $\boldsymbol{p}(t)$, such that the following condition along with the optimal trajectory $\boldsymbol{x}^*(t)$ must be satisfied for all $t \in [t_0, t_f]$:

$$\begin{cases} \dot{\boldsymbol{x}}^*(t) = \frac{\partial \mathcal{H}}{\partial \boldsymbol{p}}(\boldsymbol{x}^*(t), \boldsymbol{u}^*(t), \boldsymbol{p}^*(t), t), \\ \dot{\boldsymbol{p}}^*(t) = -\frac{\partial \mathcal{H}}{\partial \boldsymbol{x}}(\boldsymbol{x}^*(t), \boldsymbol{u}^*(t), \boldsymbol{p}^*(t), t), \\ 0 = \frac{\partial \mathcal{H}}{\partial \boldsymbol{u}}(\boldsymbol{x}^*(t), \boldsymbol{u}^*(t), \boldsymbol{p}^*(t), t), \end{cases} \tag{20}$$

and

$$\left[\frac{\partial h}{\partial \boldsymbol{x}}(\boldsymbol{x}^*(t_f), t_f) - \boldsymbol{p}^*(t_f)\right]^T \delta \boldsymbol{x}_f + \left[\mathcal{H}(\boldsymbol{x}^*(t_f), \boldsymbol{u}^*(t_f), \boldsymbol{p}^*(t_f), t_f) + \frac{\partial h}{\partial t}(\boldsymbol{x}^*(t_f), t_f)\right] \times \delta t_f = 0, \tag{21}$$

where the symbol $*$ refers to the extremals of $\boldsymbol{x}(t)$, $\boldsymbol{u}(t)$ and $\boldsymbol{p}(t)$ in Eqs. (20) and (21). Because the final state is fixed, $\delta \boldsymbol{x}_f = 0$. Hence, Eq. (21) becomes

$$\mathcal{H}(\boldsymbol{x}^*(t_f), \boldsymbol{u}^*(t_f), \boldsymbol{p}^*(t_f), t_f) + \frac{\partial h}{\partial t}(\boldsymbol{x}^*(t_f), t_f) = 0. \tag{22}$$

3.4. Necessary conditions for optimality for P2

As in the last section, by using the Hamiltonian function and Pontryagin's minimum principle equation (18) and (20), the governing equation of optimality is derived. According to Eq. (17), the final boundary condition is obtained as

$$\mathcal{H}(\boldsymbol{x}^*(t_f), \boldsymbol{u}^*(t_f), \boldsymbol{p}^*(t_f), t_f) + \frac{\partial h}{\partial t}(\boldsymbol{x}^*(t_f), t_f) + \left[\frac{\partial h}{\partial \boldsymbol{x}}(\boldsymbol{x}^*(t_f), t_f) - \boldsymbol{p}^*(t_f)\right]^T \left[\frac{d\boldsymbol{m}}{dt}(t_f)\right] = 0, \tag{23}$$

where the derivation of the last term is calculated numerically to avoid the inverse kinematics of the robot being solved.

3.5. Boundary-value problem with free end

To solve Eq. (20), the third row of Eq. (20) is substituted into the first and second rows, and the new variable $y(t)$ is defined as follows:

$$\boldsymbol{y}(t) = [\boldsymbol{x}(t), \boldsymbol{p}(t)]^T \in \mathbb{R}^{4n}, \tag{24}$$

where

$$\dot{\boldsymbol{y}}(t) = [\dot{\boldsymbol{x}}(t), \dot{\boldsymbol{p}}(t)]^T = \left[\frac{\partial \mathcal{H}}{\partial \boldsymbol{p}}, -\frac{\partial \mathcal{H}}{\partial \boldsymbol{x}}\right]^T = \boldsymbol{l}(\boldsymbol{y}(t), t), \tag{25}$$

https://doi.org/10.1017/S0263574713000362 Published online by Cambridge University Press

which satisfies the vector constraint $\boldsymbol{r} \in \mathbb{R}^{4n+1}$

$$\boldsymbol{r}(\boldsymbol{y}(t_0),\, \boldsymbol{y}(t_f)) = 0, \tag{26}$$

where the first eight rows of the $\boldsymbol{r}$ present the boundary condition (see Eqs. (12) or (16) and (17)), and the last one presents the condition of the final time (see Eqs. (22) or (23)). Instead of the time variable t, the new independent variable $0 \le \xi \le 1$ is defined as[24]

$$\xi = \frac{t - t_0}{z_{4n+1}}, \tag{27}$$

where z_{4n+1} is a positive constant. By choosing a new vector $z = [\boldsymbol{y}(t),\, z_{4n+1}]^T \in \mathbb{R}^{4n+1}$, the derivative of z with respect to ξ becomes

$$\begin{aligned} z'(\xi) &= \frac{dz(\xi)}{d\xi} = \frac{dz(t)}{dt}\frac{dt}{d\xi} = z_{4n+1}\frac{d}{dt}([\boldsymbol{y}(t),\, z_{4n+1}]^T) \\ &= z_{4n+1}[\boldsymbol{l}(z(\xi),\, t_0 + \xi z_{4n+1}),\, 0]^T. \end{aligned} \tag{28}$$

Therefore, solving $4n$ orders differential equations (25) with boundary conditions (26), is changed to $4n+1$ orders differential equations,

$$\begin{bmatrix} z_1' \\ \vdots \\ z_{4n}' \\ z_{4n+1}' \end{bmatrix} = \begin{bmatrix} z_{4n+1} l_1(z_1, \ldots, z_{4n},\, t_0 + \xi z_{4n+1}) \\ \vdots \\ z_{4n+1} l_{4n}(z_1, \ldots, z_{4n},\, t_0 + \xi z_{4n+1}) \\ 0 \end{bmatrix} \tag{29}$$

with $4n+1$ boundary conditions as below:

$$\begin{aligned} &r_i(z_1(0), \ldots, z_{4n}(0), z_1(1), \ldots, z_{4n}(1)) = 0, \\ &\quad i = 1, 2, \ldots, 4n+1. \end{aligned} \tag{30}$$

The "multiple shooting" method is used to numerically solve Eq. (29) with the boundary conditions of Eq. (30) in the interval of $0 \le \xi \le 1$. When the differential equations are solved, the parameter z_{4n+1} represents the final time t_f.

3.6. Simulation results for P1

The simulation results for P1 are shown in Fig. 3, with parameters mentioned in Table I, and $\boldsymbol{R}1 = \boldsymbol{R}2 = \boldsymbol{R}3 = \boldsymbol{I}_{2\times 2}$, $K = 1$. This choice of design parameter results in equal weighting for important criteria. In this simulation, the positions of the initial and target bars are $[-0.34, -0.015]$ and $[+0.23, +0.12]$ (m), respectively. The optimal control input $\tau(t)$ is the exerted torque to link 2 from link 1 and it is produced by the central actuator. In this problem, the variables z at the initial and final time are

$$\begin{aligned} z_0 = [&-0.6628 \quad -1.7278 \quad 0 \quad 0 \quad +0.2220 \quad +0.0601 \\ &-0.0411 \quad -0.0090 \quad +0.6439]^T, \\ z_f = [&+0.9988 \quad +2.1057 \quad 0 \quad 0 \quad -0.3243 \quad -0.0111 \\ &+0.0274 \quad +0.0008 \quad +0.6439]^T. \end{aligned} \tag{31}$$

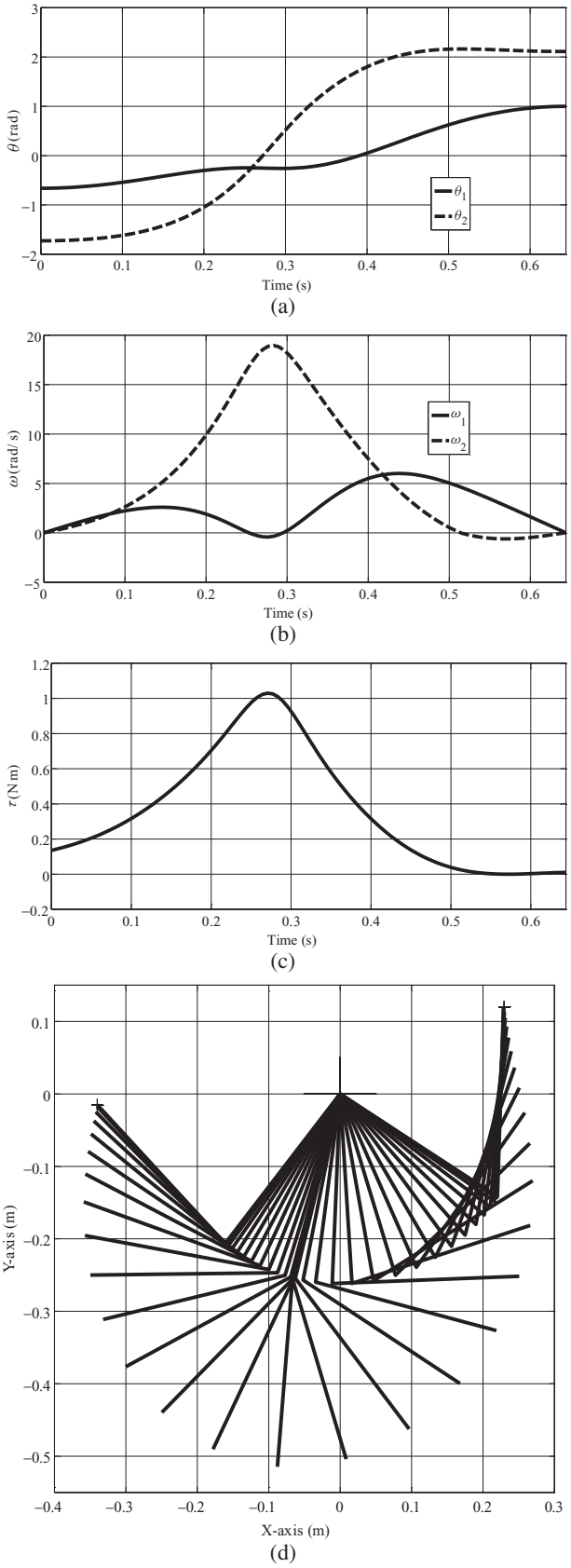


Fig. 3. Optimal simulation results of P1. The positions of the initial and target bars are $[-0.34, -0.015]$ and $[+0.23, +0.12]$ (m), respectively. (a) Joint angle; (b) joint angular velocity; (c) optimal control input; (d) movement of the brachiation robot.

https://doi.org/10.1017/S0263574713000362 Published online by Cambridge University Press

Table II. Variation of the final time with respect to the variation of K for the symmetric bar position with intervals of 0.3 m.

K	0.00	0.01	0.10	1	10	100
t_f (s)	0.6586	0.6586	0.6586	0.6582	0.6546	0.6472

The final time t_f for this problem is $z_{4n+1} = 0.6439$ (s). From the simulation results, it can be seen that the final joints angular velocities are zero; $z_{f3} = z_{f4} = 0\left(\frac{\text{rad}}{s}\right)$.

To examine the effect of the variation of the final time with respect to the variation of parameter K, a new configuration is defined based on the P1. In this simulation, the position of the initial and target bars is symmetric and the intervals between the handholds are 0.3 (m). The results are shown in Table II.

3.7. Comparing results of symmetric P1 with prior studies

As mentioned before, the "target dynamics" method is a feed-forward controller like the controller strategy derived in P1. In this section, the results of the "target dynamics" method, which was proposed by Nakanishi *et al.*[16], and the optimal method for a symmetric bar position with intervals of 0.2 (m) and $K = 1$, are presented and shown in Fig. 4. At first, the "virtual frequency" is obtained with respect to the numerical solution presented in ref. [19]. Then, the simulation results are derived based on the "target dynamics" method.[16] The "virtual frequency" for an interval of 0.2 (m) is $\omega^*(0.2) = 4.4794$ (rad/s).

3.8. Simulation results for P2

In this section, it is assumed that the target bar is moving on a known path. To show the effectiveness of this method, the trajectory of the target bar is assumed as a circle and its position as a function of time is

$$\boldsymbol{m}(t) = [0.3 - 0.1\cos(2t), 0.1\sin(2t)]^T. \tag{32}$$

The simulation results for P2 are shown in Fig. 5 with parameters mentioned in Table I, and $\boldsymbol{R}1 = \boldsymbol{R}2 = \boldsymbol{R}3 = \boldsymbol{I}_{2\times 2}$, $K = 1$. The position of the initial bar is $[-0.3, 0]$ (m).

4. Controller for Trajectory Tracking

This section presents two different controllers to track the desired trajectory for a brachiation robot. The objective mentioned in this paper has been to track the desired optimal trajectory in the system which has uncertainty in kinematic and dynamic parameters. The feed-forward controller by itself, which is mentioned in Section 3, is not applicable to the experimental brachiation robot due to the existence of disturbance and uncertainty in the system's model. Hence, two kinds of controllers, PD and AR, were investigated for tracking the proposed trajectories. At first, the previous paper on an AR set-point controller[25] is modified to make it suitable for a tracking controller. Then, the PD controller was also tuned to track the desired trajectory. The performance of these two controllers is compared in this section to select a suitable controller for experimental results.

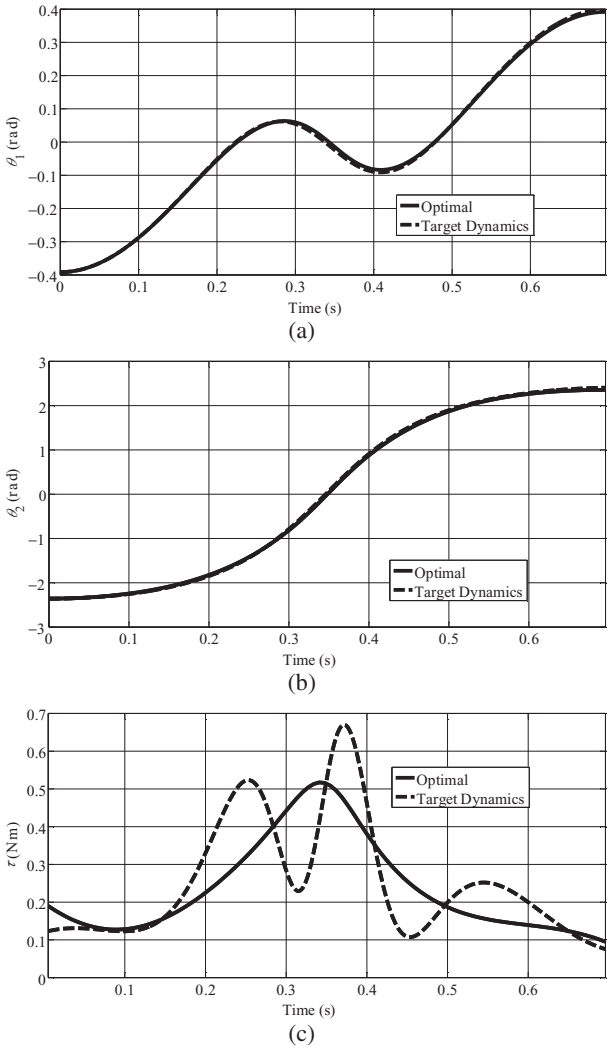


Fig. 4. Comparison of simulation results of symmetric P1 with "target dynamics" methods, for symmetric handhold position with intervals of 0.2 (m).[16] (a) First joint angle; (b) second joint angle; (c) control input.

4.1. Design of the adaptive robust controller

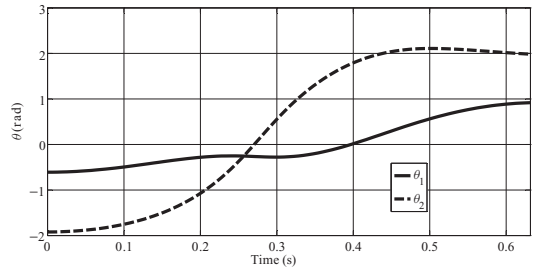
In this section, the AR set-point controller[25] is modified to become suitable for tracking controller purposes. If only $m < n$ joints of the system are equipped with actuators, the vector of a generalized coordinate can be partitioned as $\boldsymbol{q} = [\boldsymbol{q}_u, \boldsymbol{q}_a]^T$, where the index u represents the unactuated joints and the index a represents the actuated joints. The dynamic model equation (3) can be considered as

$$\begin{bmatrix} \boldsymbol{M}_{uu} & \boldsymbol{M}_{ua} \\ \boldsymbol{M}_{au} & \boldsymbol{M}_{aa} \end{bmatrix} \begin{bmatrix} \ddot{\boldsymbol{q}}_u \\ \ddot{\boldsymbol{q}}_a \end{bmatrix} + \begin{bmatrix} \boldsymbol{C}_{uu} & \boldsymbol{C}_{ua} \\ \boldsymbol{C}_{au} & \boldsymbol{C}_{aa} \end{bmatrix} \begin{bmatrix} \dot{\boldsymbol{q}}_u \\ \dot{\boldsymbol{q}}_a \end{bmatrix} + \begin{bmatrix} \boldsymbol{G}_u \\ \boldsymbol{G}_a \end{bmatrix} + \begin{bmatrix} \boldsymbol{D}_u \\ \boldsymbol{D}_a \end{bmatrix} = \begin{bmatrix} 0 \\ \boldsymbol{\tau} \end{bmatrix}. \tag{33}$$

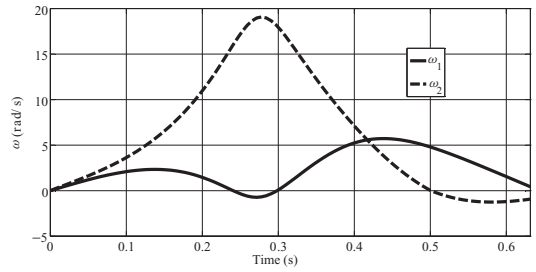
To track the desired trajectory, the difference between the actual state $\boldsymbol{q}(t)$ and the desired state $\boldsymbol{q}_d(t)$ of the system is considered as

$$\tilde{\boldsymbol{q}} = \boldsymbol{q} - \boldsymbol{q}_d. \tag{34}$$

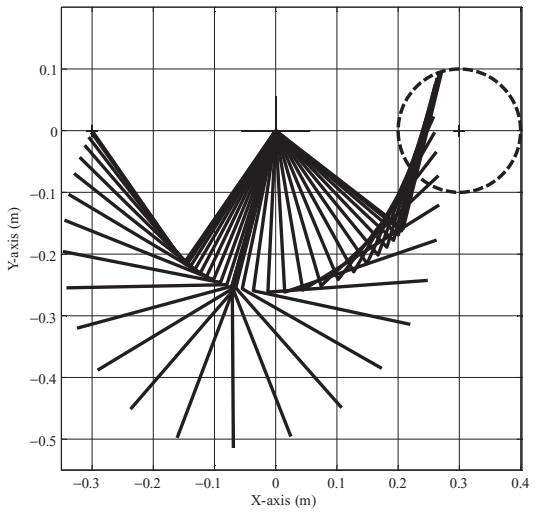
https://doi.org/10.1017/S0263574713000362 Published online by Cambridge University Press



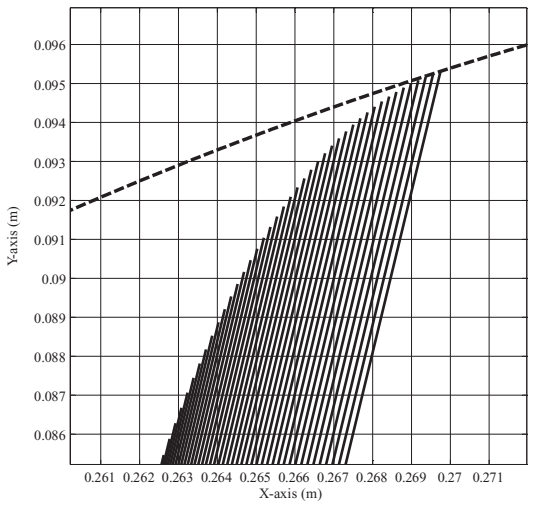
(a)



(b)



(c)



(d)

Fig. 5. Optimal simulation results of P2. The position of the initial bar is $[-0.3, 0]$ (m), and the target bar moves on the circle $[0.3 - 0.1\cos(2t), 0.1\sin(2t)]^T$ (m). (a) Joint angle; (b) joint angular velocity; (c) movement of the brachiation robot; (d) zoomed view of Fig. 5(c), when the end-effector comes into contact with the target bar.

In other words, $\tilde{\boldsymbol{q}}$ is an error surface. Variables $\boldsymbol{\mathcal{V}}$ and $\boldsymbol{\mathcal{S}}$ are defined as

$$\begin{aligned} \boldsymbol{\mathcal{V}} &= \dot{\boldsymbol{q}}_d - \boldsymbol{\Lambda}\tilde{\boldsymbol{q}}, \\ \boldsymbol{\mathcal{S}} &= \dot{\tilde{\boldsymbol{q}}} + \boldsymbol{\Lambda}\tilde{\boldsymbol{q}}, \end{aligned} \tag{35}$$

where $\boldsymbol{\Lambda}$ is a positive-definite matrix and the vector $\boldsymbol{\mathcal{S}}$ resembles the sliding surface. Choose the input control law as follows:

$$\boldsymbol{\tau} = \boldsymbol{\Phi}_a\hat{\boldsymbol{\alpha}}_a + \boldsymbol{\mathcal{J}}_a\boldsymbol{\mathcal{S}}_a + \boldsymbol{\tau}_0, \tag{36}$$

where $\boldsymbol{\Phi}_a$ is a matrix of known functions of generalized coordinates and generalized velocities. $\boldsymbol{\alpha}_a$ is an unknown constant vector of the system parameters appeared in actuated rows of Eq. (33) and $\hat{\boldsymbol{\alpha}}_a$ is an estimate for $\boldsymbol{\alpha}_a$. The matrix $\boldsymbol{\mathcal{J}} = \mathrm{diag}([\boldsymbol{\mathcal{J}}_u, \boldsymbol{\mathcal{J}}_a])$ where $\boldsymbol{\mathcal{J}}_u, \boldsymbol{\mathcal{J}}_a > 0$ and $\boldsymbol{\tau}_0$ are design parameters. Substituting Eq. (36) in Eq. (33) results in

$$\boldsymbol{M}\dot{\boldsymbol{\mathcal{S}}} + \boldsymbol{C}\boldsymbol{\mathcal{S}} + \boldsymbol{\mathcal{J}}\boldsymbol{\mathcal{S}} = \begin{bmatrix} -\boldsymbol{\Phi}_u\boldsymbol{\alpha}_u + \boldsymbol{\mathcal{J}}_u\boldsymbol{\mathcal{S}}_u \\ -\boldsymbol{\Phi}_a\boldsymbol{\alpha}_a + \boldsymbol{\tau}_0 \end{bmatrix} + \boldsymbol{d}(t), \tag{37}$$

where $\boldsymbol{d}(t)$ is a bounded vector of disturbance including unmodeled dynamics of the system. $\boldsymbol{\alpha}_u$ is a constant vector of the system parameters appeared in unactuated rows of Eq. (33) and $\boldsymbol{\Phi}_u$ is a matrix which is a function of generalized coordinates and generalized velocities that are already known. $\tilde{\boldsymbol{\alpha}}_a$ denotes the difference between actual and estimated values of the parameter $\boldsymbol{\alpha}_a$. In Eq. (37), the values of $\boldsymbol{\alpha}_a$, $\boldsymbol{\alpha}_u$, $\boldsymbol{\Phi}_a$ and $\boldsymbol{\Phi}_u$ are

$$\begin{aligned} \boldsymbol{\alpha}_a &= [\, a_2 \quad a_3 \quad b_2 \quad I_m \quad c_2 \quad \boldsymbol{v}_2 \,]^T, \\ \boldsymbol{\alpha}_u &= [\, a_1 \quad a_2 \quad a_3 \quad b_1 \quad b_2 \quad c_1 \quad \boldsymbol{v}_1 \,]^T, \\ \boldsymbol{\Phi}_a &= \big[\dot{\boldsymbol{\mathcal{V}}}_a + \dot{\boldsymbol{\mathcal{V}}}_u \quad \cos(q_2)\dot{\boldsymbol{\mathcal{V}}}_{\boldsymbol{u}} \\ &\qquad + \sin(q_2)\dot{q}_1\boldsymbol{\mathcal{V}}_u \quad \sin(q_1 + q_2) \quad \dot{\boldsymbol{\mathcal{V}}}_a \quad \mathrm{sign}(\dot{q}_2) \quad \dot{q}_2\big], \\ \boldsymbol{\Phi}_u &= \big[\dot{\boldsymbol{\mathcal{V}}}_u \quad \dot{\boldsymbol{\mathcal{V}}}_a + \dot{\boldsymbol{\mathcal{V}}}_u \quad 2\cos(q_2)\dot{\boldsymbol{\mathcal{V}}}_u + \cos(q_2)\dot{\boldsymbol{\mathcal{V}}}_a \\ &\qquad -\sin(q_2)\,\dot{q}_2\boldsymbol{\mathcal{V}}_u - \sin(q_2)(\dot{q}_1 + \dot{q}_2)\boldsymbol{\mathcal{V}}_a \quad \sin(q_1) \\ &\qquad \sin(q_1 + q_2) \quad \mathrm{sign}(\dot{q}_1) \quad \dot{q}_1\big]. \end{aligned} \tag{38}$$

For the stability analysis of the system, the Lyapunov function is considered as

$$\mathbb{V} = \frac{1}{2}\boldsymbol{\mathcal{S}}^T\boldsymbol{M}\boldsymbol{\mathcal{S}} + \frac{1}{2}\tilde{\boldsymbol{\alpha}}_a^T\boldsymbol{\Gamma}^{-1}\tilde{\boldsymbol{\alpha}}_a, \tag{39}$$

where $\boldsymbol{\Gamma}$ is a positive-definite matrix. The derivation of the Lyapunov function with respect to time is

$$\begin{aligned} \dot{\mathbb{V}} = &-\boldsymbol{\mathcal{S}}^T\boldsymbol{\mathcal{J}}\boldsymbol{\mathcal{S}} + \frac{1}{2}\mathcal{S}^T(\dot{\boldsymbol{M}} - 2\boldsymbol{C})\boldsymbol{\mathcal{S}} + \left(\dot{\tilde{\boldsymbol{\alpha}}}_a^T\boldsymbol{\Gamma}^{-1} - \boldsymbol{\mathcal{S}}_u^T\boldsymbol{\Phi}_a\right)\tilde{\boldsymbol{\alpha}}_a \\ &+ \boldsymbol{\mathcal{S}}_u^T(\boldsymbol{\mathcal{J}}_u\boldsymbol{\mathcal{S}}_u - \boldsymbol{\Phi}_u\boldsymbol{\alpha}_u) + \boldsymbol{\mathcal{S}}_a^T\boldsymbol{\tau}_0 + \boldsymbol{\mathcal{S}}^T\boldsymbol{d}(t), \end{aligned} \tag{40}$$

where the first term is negative definite. The second term is obviously equal to zero because the matrix $\dot{\boldsymbol{M}}(\boldsymbol{q}) - 2\boldsymbol{C}(\boldsymbol{q}, \dot{\boldsymbol{q}})$ is skew-symmetric. Here, $\dot{\tilde{\boldsymbol{\alpha}}}_a$ is considered to adaptively

https://doi.org/10.1017/S0263574713000362 Published online by Cambridge University Press

vanish the third term:

$$\dot{\hat{\boldsymbol{\alpha}}}_a = \boldsymbol{\Gamma}^T \boldsymbol{\Phi}_a^T \boldsymbol{\mathcal{S}}_a \tag{41}$$

and $\boldsymbol{\tau}_0$ is set as

$$\boldsymbol{\tau}_0 = -\gamma \frac{\boldsymbol{\mathcal{S}}_a}{\|\boldsymbol{\mathcal{S}}_a\|^2 + \varepsilon}, \tag{42}$$

where $\varepsilon > 0$ is a small constant and

$$\gamma = \boldsymbol{\mathcal{S}}_u^T \boldsymbol{\mathcal{J}}_u \boldsymbol{\mathcal{S}}_u + \left\| \boldsymbol{\mathcal{S}}_u^T \boldsymbol{\Phi}_u \right\| \rho_{\boldsymbol{\alpha}_u} + \|\boldsymbol{\mathcal{S}}\| \, \rho_{\boldsymbol{d}(t)}, \tag{43}$$

where $\|\|$ is the norm of the vector, and ρ_{α_u} and $\rho_{d(t)}$ are the known maximum bound of vectors $\boldsymbol{\alpha}_u$ and $\boldsymbol{d}(t)$, respectively. Thus,

$$\|\boldsymbol{\alpha}_u\| < \rho_{\boldsymbol{\alpha}_u}, \|\boldsymbol{d}(t)\| < \rho_{\boldsymbol{d}(t)}. \tag{44}$$

With the above statements in mind, by substituting Eqs. (42) and (43) into Eq. (40), the derivation of the Lyapunov function becomes

$$\begin{aligned} \dot{\mathbb{V}} = & -\boldsymbol{\mathcal{S}}^T \boldsymbol{\mathcal{J}} \boldsymbol{\mathcal{S}} + \frac{\|\boldsymbol{\mathcal{S}}_a\|^2}{\|\boldsymbol{\mathcal{S}}_a\|^2 + \varepsilon} \left(\boldsymbol{\mathcal{S}}_u^T \boldsymbol{\mathcal{J}}_u \boldsymbol{\mathcal{S}}_u + \left\| \boldsymbol{\mathcal{S}}_u^T \boldsymbol{\Phi}_u \right\| \rho_{\boldsymbol{\alpha}_u} \right. \\ & \left. + \|\boldsymbol{\mathcal{S}}\| \, \rho_{\boldsymbol{d}(t)} \right) + \boldsymbol{\mathcal{S}}_u^T (\boldsymbol{\mathcal{J}}_u \boldsymbol{\mathcal{S}}_u - \boldsymbol{\Phi}_u \boldsymbol{\alpha}_u) \\ & + \boldsymbol{\mathcal{S}}^T \boldsymbol{d}(t) \leq -\boldsymbol{\mathcal{S}}^T \boldsymbol{\mathcal{J}} \boldsymbol{\mathcal{S}}. \end{aligned} \tag{45}$$

The $\dot{\mathbb{V}}$ is negative semi-definite. Hence, the Lyapunov function and the error of estimation are bounded. In other words, $\boldsymbol{\mathcal{S}} \in L_\infty$ and $\tilde{\boldsymbol{\alpha}}_a \in L_\infty$. From Eq. (45), one can directly observe that $\boldsymbol{\mathcal{S}} \in L_2$, and from Eq. (37) it can be seen that $\dot{\boldsymbol{\mathcal{S}}}$ is also bounded, which means $\dot{\boldsymbol{\mathcal{S}}} \in L_\infty$. Using Barbalat's lemma infers that $\lim_{t \to \infty} \boldsymbol{\mathcal{S}}(t) = 0$. Therefore, it can be concluded that $\lim_{t \to \infty} \tilde{\boldsymbol{q}}(t) = 0$ and, as a result, $\lim_{t \to \infty} \boldsymbol{q}(t) = \boldsymbol{q}_d(t)$.

4.2. Design of the PD controller

In this section, a PD controller is designed to track the desired trajectory. The control input torque is considered as

$$\tau = \tau_{\text{Optimal}} + \tau_{\text{feedback}}, \tag{46}$$

where τ_{optimal} is the feed-forward input torque obtained from optimal theory (P1 or P2), and τ_{feedback} is a tuned PD controller used to track the desired trajectories (P1 or P2) and is considered as

$$\begin{aligned} \tau_{\text{feedback}} = & \begin{bmatrix} k_{P1} & k_{P2} \end{bmatrix} \begin{bmatrix} \theta_{1\text{Optimal}} - \theta_1 \\ \theta_{2\text{Optimal}} - \theta_2 \end{bmatrix} \\ & + \begin{bmatrix} k_{D1} & k_{D2} \end{bmatrix} \begin{bmatrix} \dot{\theta}_{1\text{Optimal}} - \dot{\theta}_1 \\ \dot{\theta}_{2\text{Optimal}} - \dot{\theta}_2 \end{bmatrix}, \end{aligned} \tag{47}$$

where k_{Pi} and k_{Di}, $i = 1, 2$ are constant.

4.3. Simulation conditions for the PD and adaptive robust controller

In this section, the simulation conditions for the PD and AR controllers are presented. Due to model uncertainties and measurement accuracy, the actual parameters of the CEDRA brachiation robot defer from the parameters listed in Table I (measured parameters). Therefore, different sets of parameters called "simulation parameters" shown in Table III (assuming to be actual) are used for simulation purposes. Furthermore, the optimal trajectories are obtained by using the parameters mentioned in Table I. However, the objective here for the system with the parameters listed in Table III was to track the obtained trajectories. In fact, this method shows the ability of the controller to track the desired trajectory for a system with significant uncertainties. It can be observed from Tables I and III that the uncertainty is about 15% and it is also assumed that $d(t) = [0.05 \sin(\dot{\theta}_1), 0.05 \sin(\dot{\theta}_2)]^T$ as the unmodeled dynamics.

Table III. Kinematic and dynamic parameters of the brachiation robot for the simulation of the tracking controller.

Symbol (unit)	$i = 1$	$i = 2$
m_i (kg)	0.4	1.2
l_i (m)	0.262	0.262
l_{ci} (m)	0.15	0.08
I_i^c (kg m^2)	$4.6e-3$	$11.6e-3$
c_i (N m)	0.01	0.1
ν_i (N m s)	0.01	0.03
I_m (kg m^2)	$2.2e-3$	

The tuned design parameters for an AR controller are

$$\boldsymbol{\Lambda} = \begin{bmatrix} 0.3 & 0 \\ 0 & 0.5 \end{bmatrix}, \quad \boldsymbol{\Gamma} = \text{diag}([1, 1, 1, 1, 1, 1])$$

$$\boldsymbol{\mathcal{J}} = \begin{bmatrix} 0.1 & 0 \\ 0 & 0.3 \end{bmatrix}, \quad \varepsilon = 0.1, \quad \rho_{\boldsymbol{\alpha}_u} = 4, \quad \rho_{\boldsymbol{d}(t)} = 0.1. \tag{48}$$

The simulation conditions for the PD controller are as those discussed earlier. However, the tuned design parameters for the PD controller are

$$\boldsymbol{k}_P = [1 \; 5], \quad \boldsymbol{k}_D = [0 \; 2]. \tag{49}$$

4.4. Comparison of simulation results of the PD with an adaptive robust controller

In order to compare the performance of the two proposed methods, the results of the PD and AR controllers are jointly illustrated in Fig. 6.

The joints angle and velocity are almost the same as for the PD and AR controllers. Therefore, the tracking errors are compared as well. It can be seen from Fig. 6(c) that the errors oscillate around zero. This is because of an inadequate brachiation time for the controllers to settle. The two controllers have almost the same performance, although the PD minimizes the distance between the end-effector and the target bar (0.7 mm) in comparison with an AR controller (4 mm).

The control input of the PD and AR controllers is shown in Fig. 6(d). Two kinds of ripples or chattering, namely low-frequency ripple and high-frequency ripple, exist in the control effort. The low-frequency ripple, which exists in both

https://doi.org/10.1017/S0263574713000362 Published online by Cambridge University Press

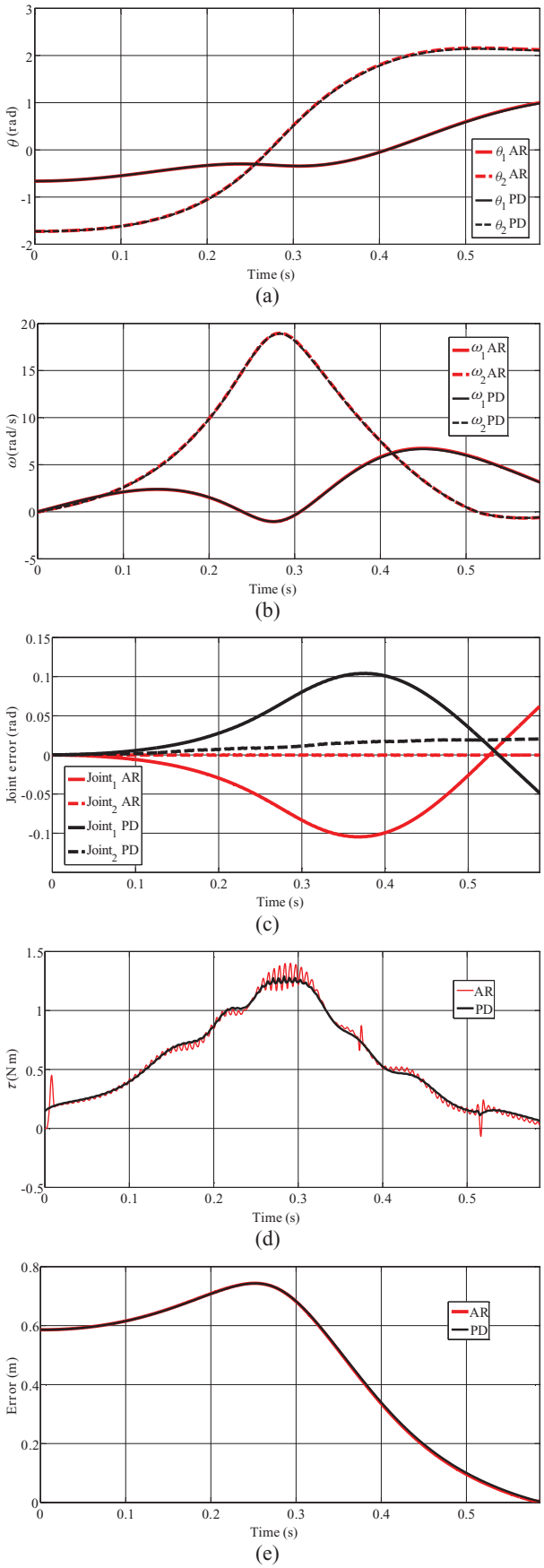


Fig. 6. (Colour online) Comparison of simulation results of the PD with an AR controller for obtained trajectory in P1. (a) Joint angle; (b) joint angular velocity; (c) joint tracking error; (d) control input; (e) distance between the end-effector and the target bar.

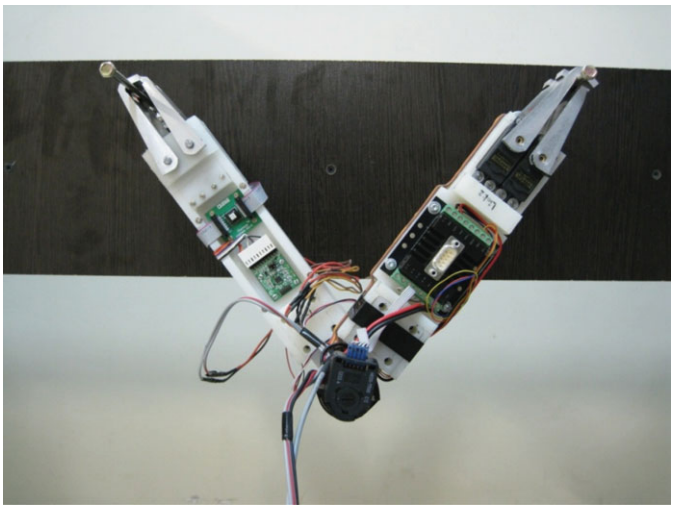


Fig. 7. (Colour online) The CEDRA two-link brachiation robot.

control efforts, is a consequence of unmodeled dynamics of the brachiation robot. On the other hand, the high-frequency chattering is the consequence of the sliding mode nature of an AR controller.

5. Experimental Testbed

5.1. Physical apparatus

This section describes the experimental setup of the brachiation robot which is used to validate the proposed control strategy. The configuration of the CEDRA brachiation robot is illustrated in Fig. 7. The CEDRA brachiation robot has two links and two grippers at the end of each link. In order to grab the target bar, each gripper is equipped with two radio-controlled (RC) servo motors. It should be noted that the gripper actuators do not work on the system. A direct current (DC) coreless motor is placed at the central joint as the only actuator of the robot. The DC motor (3868A024C), gearbox (38/2S14:1), encoder (HEDS5500C12) and motion controller (MCDC3006S) with the ability of torque control are produced by the "Faulhaber" group. The exerted torque of the DC motor is

$$\tau = K_m \boldsymbol{i}, \tag{50}$$

where K_m is the torque constant and equals 33.3 (mN m/A), and i is input current to the motor.

To measure the angle between links 1 and 2, an encoder is attached to the motor's shaft. As it is impossible to measure the absolute angle of link 1 with an encoder or a potentiometer, a gyroscope sensor (InvenSense Inc., ISZ-650EVB) and an inclinometer (Analog Devices Inc., ADIS16209/PCBZ) are attached to the first link to measure the angular velocity and angular position, respectively. A combination of the signals obtained from the gyroscope and the inclinometer is used to estimate the accurate angle of the first link.[26]

https://doi.org/10.1017/S0263574713000362 Published online by Cambridge University Press

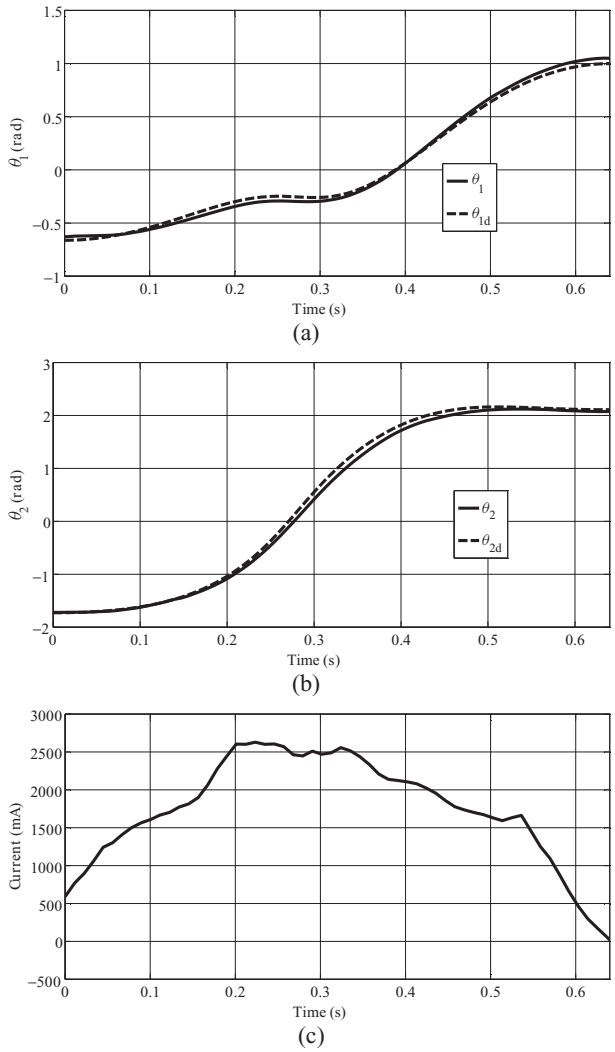


Fig. 8. Experimental results of the PD tracking controller for obtained trajectories in P1 for the CEDRA brachiation robot. (a) First joint angle; (b) second joint angle; (c) input current to the central actuator.

5.2. *Experimental results*

According to theoretical results, the PD controller has shown better performance than the AR controller due to the no chattering phenomenon and low computational efforts. High-frequency oscillation called chattering is an inherent characteristic of such a controller like sliding mode controller. On the other hand, the sample time of the motion controller (MCDC3006S) in current control mode is 100 (Hz). Therefore, the experimental results are obtained using the PD action controller to track the designed trajectory. The experimental results of the PD tracking controller for obtained trajectory in P1 for the CEDRA brachiation robot are shown in Fig. 8. The positions of the initial and target bars are $[-0.34, -0.015]$ and $[+0.23, +0.12]$ (m), respectively. The design parameters are

$$\boldsymbol{k}_P = [\,0.6\ 3.5\,],\ \boldsymbol{k}_D = [\,0.0\ 0.9\,]. \tag{51}$$

The gripper actuator has a finite angular velocity (400 deg /s). To solve this problem, the gripper actuator is activated 50 ms just before the robot actuator begins to do work on the system. Hence, a small error is observed in the beginning of Fig. 8(a). This error exists because the first joint moves while detaching the initial bar. The undesired motion of the power cable was seen to be the most effective source of disturbance during brachiation. To reduce this effect, it is recommended to use a battery or a very light flexible cable.

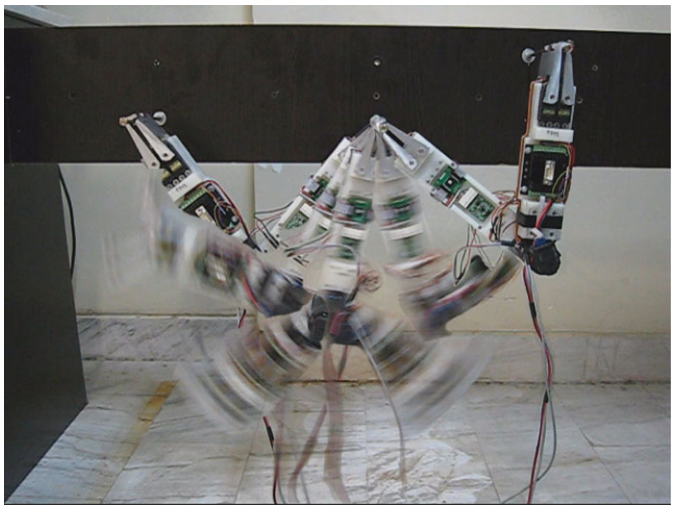


Fig. 9. (Colour online) The movement of the CEDRA brachiation robot with the PD tracking controller for obtained trajectory in P1.

As one can observe in Figs. 8(b) and (c), the maximum current is applied where θ_2 is close to zero, where in this neighborhood some ripples exist due to the sign change of the angular acceleration of the second joint and the backlash in the gearbox.

As mentioned before, the angular velocity of the gripper is limited and it will take about 200 ms for the gripper to rotate 90° . To overcome this problem, the grabbing command is sent when the end-effector enters into the neighborhood of the target bar, and just before the gripper touches it.

The movement of the CEDRA brachiation robot with a PD tracking controller for trajectories obtained in P1 is shown in Fig. 9.

6. Conclusion and Future Works

This paper presents control issues of the CEDRA brachiation robot that moves from one branch to another like a long-armed ape. Here, Pontryagin's minimum principle is used to obtain the optimal trajectories, which lead the robot to brachiate on completely irregular branches. This theory guarantees global optimality for the case where a positive-definite performance criterion is selected. The irregularity in branches can be in distance and height. The previous method on the set-point controller for an acrobat robot is improved to represent an AR servo controller to ensure that the system tracks the desired trajectory.[25] This controller has the capability to be used in systems that have uncertainty in both kinematic and dynamic parameters. Theoretical results indicate that the control effort is reduced by 25% in comparison with the "target dynamics" method, which was proposed in prior papers for such a robot.[16] The brachiation time is an inherent characteristic of the system dynamics and it also depends on the initial and final conditions, so it

https://doi.org/10.1017/S0263574713000362 Published online by Cambridge University Press

cannot be improved significantly (see Table II). Two kinds of controllers, the PD and the AR, were investigated for tracking the proposed trajectories. The theoretical results are shown and validated with experimental observations. Numerical simulations and experimental results illustrate the effectiveness of the proposed method. Future works can be listed as follows:

(1) *Ricochetal brachiation*. This problem involves the fast swing and investigation of the motion of the long-armed ape in the air.
(2) *Flexible bar*. In this problem, the supporting bar is assumed to be flexible and deform significantly under loading.

Acknowledgments

The author would like to thank Dr. Mehrzad Namvar (Department of Electrical Engineering of the Sharif University of Technology) for his guidance and valuable suggestions in developing the control law.

References

1. J. Nakanishi, T. Fukuda and D. E. Koditschek, "Preliminary Studies of a Second Generation Brachiation Robot Controller," *Proceedings of the IEEE International Conference on Robotics and Automation*, Albuquerque, NM, USA (1997) pp. 2050–2056.
2. T. Fukuda, H. Hosokai and Y. Kondo, "Brachiation Type of Mobile Robot," *Proceedings of the Fifth International Conference on Advanced Robotics,* Robots in Unstructured Environments, vol. 2, Pisa, Italy, (1991) pp. 915–920.
3. V. M. De Oliveira and W. F. Lages, "MPC Applied to Motion Control of an Underactuated Brachiation Robot," *Proceedings of the IEEE Symposium on Emerging Technologies and Factory Automation, ETFA*, Hamburg, Germany (2006) pp. 985–988.
4. V. M. De Oliveira and W. F. Lages, "Control of a brachiating robot for inspection of aerial power lines," *Proceedings of the 1st International Conference on Applied Robotics for the Power Industry (CARPI),* Montreal, QC (2010) pp. 1–6.
5. D. Lee, T. C. Burg, D. M. Dawson, D. Shu, B. Xian and E. Tatlicioglu, "Robust tracking control of an underactuated quadrotor aerial-robot based on a parametric uncertain model," *Proceedings of the IEEE International Conference on Systems, Man and Cybernetics*, San Antonio, TX (2009) pp. 3187–3192.
6. J. R. Azinheira, A. Moutinho and E. C. De Paiva, "A backstepping controller for path-tracking of an underactuated autonomous airship," *Int. J. Robust Nonlinear Control*, **19**, 418–441 (2009).
7. W. Chen, L. Zhao, X. Zhao and Y. Yu, "Control of the underactuated flexible manipulator in the operational space," *Proceedings of the International Conference on Intelligent Human-Machine Systems and Cybernetics*, Hangzhou, Zhejiang (2009) pp. 470–473.
8. M. W. Spong, "Swing up control problem for the acrobot," *IEEE Control Syst. Mag.* **15**, 49–55 (1995).
9. M. S. Park and D. Chwa, "Swing-up and stabilization control of inverted-pendulum systems via coupled sliding-mode control method," *IEEE Trans. Ind. Electron.* **56**, 3541–3555 (2009).
10. T. Fukuda, F. Saito and F. Arai, "Study on the Brachiation Type of Mobile Robot (Heuristic creation of driving input and control using CMAC)," *Proceedings of the IEEE/RSJ International Workshop on Intelligent Robot and Systems '91*, Osaka, Japan (1991) pp. 478–483.
11. F. Saito, T. Fukuda and F. Arai, "Swing and locomotion control for a two-link Brachiation robot," *IEEE Control Syst. Mag.* **14**, 5–11 (1994).
12. F. Saito, T. Fukuda, F. Arai and K. Kosuge, "Heuristic generation of driving input and control of brachiation robot," *JSME Int. J.* **37**, 147–154 (1994).
13. M. W. Gomes and A. L. Ruina, "A five-link 2D brachiating ape model with life-like zero-energy-cost motions," *J. Theor. Biol.* **237**, 265–278 (2005).
14. H. Nishimura and K. Funaki, "Motion control of brachiation robot by using final-state control for parameter-varying systems," *Proceedings of the 35th IEEE Conference on Decision and Control*, Kobe, Japan (1996) pp. 2355–3592.
15. H. Nishimura and K. Funaki, "Motion control of three-link brachiation robot by using final-state control with error learning," *IEEE/ASME Trans. Mechatronics* **3**, 120–128 (1998).
16. J. Nakanishi, T. Fukuda and D. E. Koditschek, "Experimental Implementation of a 'Target Dynamics' Controller on a Two-Link Brachiating Robot," *Proceedings of the IEEE International Conference on Robotics and Automation*, Leuven, Belgium (1998) pp. 787–792.
17. J. Nakanishi, T. Fukuda and D. E. Koditschek, "Hybrid Swing up Controller for a Two-Link Brachiating Robot," *Proceedings of the IEEE/ASME International Conference on Advanced Intelligent Mechatronics* (1999) pp. 549–554.
18. J. Nakanishi, T. Fukuda and D. E. Koditschek, "A brachiating robot controller," *IEEE Trans. Robot. Autom.* **16**, 109–123 (2000).
19. J. Nakanishi and T. Fukuda, "Preliminary analytical approach to a brachiation robot controller," Technical report: CGR 96–08 / CSE TR 305-96, The University. of Michigan, EECS Department (1996).
20. J. Nakanishi, T. Fukuda and D. E. Koditschek, "Brachiation on a ladder with irregular intervals," *Adv. Robot.* **16**, 147–160 (2002).
21. V. M. De Oliveira and W. F. Lages, "Linear Predictive Control of a Brachiation Robot," *Proceedings of the Canadian Conference on Electrical and Computer Engineering*, Ottawa, ON (2007) pp. 1518–1521.
22. H. Baruh, *Analytical Dynamics* (McGraw-Hill, New York 1998).
23. D. E. Kirk, *Optimal Control Theory: An Introduction* (Prentice-Hall, Englewood Cliffs, NJ 1970).
24. J. Stoer and R. Bulirsch, *Introduction to Numerical Analysis*, 2nd ed. (Springer-Verlag, New York, 1980).
25. C. Y. Su and Y. Stepanenko, "Adaptive variable structure set-point control of underactuated robots," *IEEE Trans. Autom. Control* **44**, 2090–2093 (1999).
26. J. Leavitt, A. Sideris and J. E. Bobrow, "High bandwidth tilt measurement using low cost sensors," *Mechatronics, IEEE/ASME Trans.* vol. 11, pp. 320–327, (2006).

https://doi.org/10.1017/S0263574713000362 Published online by Cambridge University Press